

Three dimensional cluster distributions in processed multi-wall carbon nanotube polymer composites



Doyoung Moon^a, Jan Obrzut^a, Jack F. Douglas^a, Thomas Lam^b, Krzysztof K. Koziol^c, Kalman B. Migler^{a,*}

^aMaterials Science and Engineering Division, National Institute Standards and Technology, Gaithersburg, MD 20899, USA

^bCenter for Nanoscale Science and Technology, National Institute Standards and Technology, Gaithersburg, MD 20899, USA

^cUniversity of Cambridge, Department of Material Science & Metallurgy, Cambridge CB2 3QZ, England, UK

ARTICLE INFO

Article history:

Received 6 January 2014

Received in revised form

30 April 2014

Accepted 7 May 2014

Available online 16 May 2014

Keywords:

Nanocomposite

CNTs

Clusters

ABSTRACT

We determine the three-dimensional structure of melt-mixed carbon nanotube (CNT) networks in an amorphous polymer matrix via confocal microscopy and image analysis. We find that the CNT networks consist of ramified clusters whose size distribution scales with cluster mass according to exponents typical of percolating systems. Remarkably, these scaling relationships hold over a wide range of concentrations, processing operations (squeezing, shearing, annealing) and subsequent electrical conductivity levels. Our results suggest that the power law scaling of cluster mass with size and frequency might be an important principle governing multi-wall carbon nanotube (MWCNT) structure in processed composites. We suggest that subtle changes in MWCNT-polymer interface structure may play a significant role in composite electrical direct current DC conductivity. Also, we find that residual flow plays a key role in the phenomenon of conductivity recovery during post-process annealing.

Published by Elsevier Ltd.

1. Introduction

¹Nanocomposites composed of multi-wall carbon nanotubes (MWCNTs) in a polymer matrix can exhibit strong enhancements in electrical conductivity and potentially in mechanical [1] and thermal properties [2]. Due to the large length (L) to diameter (d) aspect ratios of the MWCNTs, (L/d from 100 to 10,000) they can form conducting networks at low volume fractions [3]. However, it is now well understood that processing operations, such as extrusion [4] and injection molding [5], can dramatically alter the nanocomposite conductivity, in some cases causing a conducting to insulating transition. An important goal of MWCNT-nanocomposite research is to develop robust processes that maximize electrical conductivity while minimizing nanotube concentration. Thus much laboratory work revolves around measurement of the interrelationships between shear rate [6], network structure (cluster dispersion) [7–9], extensional flow [10], carbon nanotube (CNT) orientation [11], annealing and the resulting properties, such as

bulk conductivity [12–15]. Earlier studies have shown that the conductivity of well dispersed CNTs in polypropylene nanocomposites decreases with increasing shear rate [6]. The applied shear field shifts the critical percolation concentration to higher CNT concentration by breaking down the CNT conducting network structure. As a result the composites undergo a conductor to insulator transition (see Eq. 6 in Ref. [6]).

An important concept to emerge recently is that the concentration of MWCNTs is not uniform throughout a sample [13,16], but rather varies, with nanotubes existing in clusters, which are strongly influenced by flow. In this case, the conductive pathways through the nanocomposite are through the clusters. Here we use the term cluster to refer to those structures which are formed by the processing that exist over a broad range of length scales. At CNT concentrations greater than the percolation point, these length scales equal the physical size of the entire sample. This is distinct from high density aggregates of nanotubes that are produced during the manufacturing process; in a successful dispersion process, these are then dispersed into the polymer melt, where the above mentioned clusters can form.

Eken et al. [7,17] show that the effect of both material properties and imposed flow on the microstructure and electrical conductivity of MWCNT/polymer composites by employing fiber-level simulation. According to their results, the shear rate influences the

* Corresponding author. Tel.: +1 301 975 4876; fax: +1 301 975 4924.

E-mail address: kalman.migler@nist.gov (K.B. Migler).

¹ Official contribution of the National Institute of Standards and Technology; not subject to copyright in the United States.

composite conductivity by facilitating the formation or destruction of conductive clusters.

Clusters that span the sample are one of two necessary ingredients for a conducting sample, the second is that the distance of closest approach between the adjacent nanotubes that define a cluster must be below a critical size to allow for electron tunneling from nanotube to nanotube [18]. We note that in our analysis, we define a single physically isolated nanotube to be a cluster containing one nanotube. During annealing operations, it has been observed that conductivity, which had been broken down during shear, can recover and there is some evidence that this is associated with nanotubes reforming clusters [13]. However since the diffusive motion of the nanotubes in the viscous polymer is quite low, the driving force causing the nanotubes to re-orient and re-configure is not established.

The measurement of the structure of the nanotube networks in a polymer matrix is necessary to develop processing conditions that optimize the nanocomposite properties. However, the network structure is inherently three-dimensional and prior works do not visualize the 3D clusters that make up these networks. Electron microscopies can probe individual tubes and small clusters, but it is difficult to image over an appreciable thickness of a 3D sample to ascertain the structure. Standard optical microscopy has not been able to resolve individual nanotubes in a way that measures their 3D networks. Efforts to probe bulk properties have utilized techniques such as optical scattering [19,20], dichroism [21] or rheology [22] that measure ensemble properties. Such information regarding 3D clusters would permit better comparison with simulations and provide insights into the reasons for the observed decrease in conductivity upon shear.

In this work, we measure the three dimensional structure of MWCNTs networks by utilizing nanotubes whose size is large enough to be resolved in a laser scanning confocal microscopy (LSCM). We employ three dimensional imaging techniques developed for fluorescence microscopy and tomography [23]. These techniques permit us to obtain and analyze 3D volumetric data and allows us to visualize and extract statistical information regarding individual nanotubes and their clusters in the percolated regime. We measure the effects of model processing steps (squeezing, shearing, annealing) on the cluster sizes, in-plane nanotube orientation and the resulting conductivity.

2. Experimental

2.1. Nanocomposite

²Our selection of carpet grown MWCNTs for the CNT and of polystyrene as the matrix was governed primarily by the requirements of the optical imaging techniques employed here. We require CNTs of sufficient diameter and length that they can be imaged in confocal optical microscopy. The choice of polymer is governed by the needs for optical transparency and that it be solid at room temperature so that the sample can be transferred from the shear cell to the confocal microscope without disturbing the nanotube network. There is also a constraint on the MWCNT concentration that stems from its optical absorption. As the concentration increases, the ability to image deeper into the sample decreases. The optical results obtained in this paper were obtained at concentrations at and below of 0.5% by mass where there is an

acceptable trade-off between conductivity and optical transparency. Optical measurements in the plateau region (corresponding to concentrations beyond the percolation point) become difficult and are not reported here.

The MWCNTs were synthesized using a method described by Singh et al. [24] based on a chemical vapor deposition technique that allows production of highly aligned “carpets” of MWCNTs. The number average length is 25 μm with a broad distribution ranging from (2.5 to 100) μm . The nanotube diameters were measured via transmission electron microscopy (TEM), (FEI Titan™ 80–300 S/TEM, at an operating voltage of 300 kV and the length is measured by digitizing the bright field confocal images of a dilute MWCNT composite (0.02% mass fraction). The number average CNT length and diameter are 25 μm and 56 nm, respectively (Fig. 1).

We prepared a series of polystyrene/MWCNT composites as our model system. A solution mixing method is used to produce the PS/MWCNT nanocomposites. First, MWCNT powder and PS pellets (PS, STYRON® 612, DOW Chemicals) are weighed and prepared with excess toluene as a solvent, and the mixture is mixed over 2 h by high speed stirring. The solvent is subsequently dried overnight. Three MWCNT samples were utilized in this work with mass fractions of 0.02%, 0.1% and 0.5% (on a per mass basis of MWCNT to polymer).

2.2. Model processing

The model processing steps were conducted in a heated parallel-plate rotating-disk shear-cell (Linkam, CSS450). As the nanotubes diffuse very little in the polymer matrix, every processing step – even sample loading – can affect the structure and

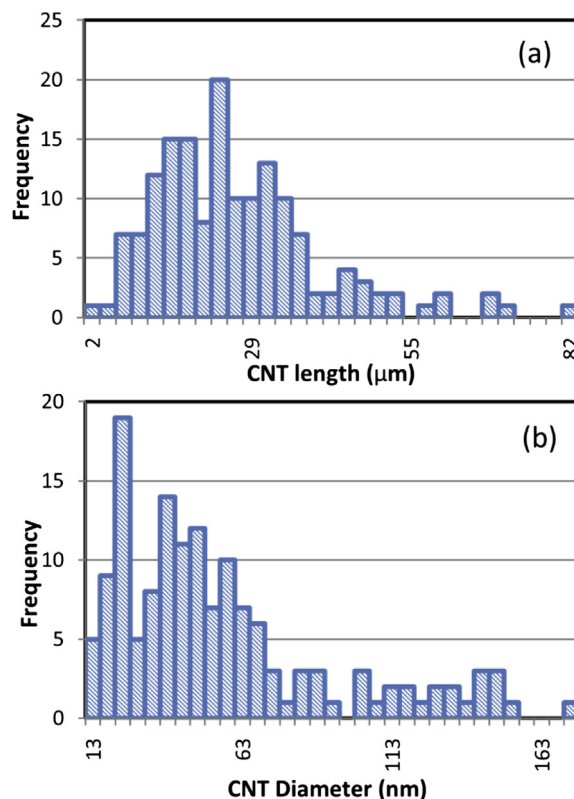


Fig. 1. Length and diameter distribution of MWCNTs used in this study as determined by confocal microscopy (a) and TEM (b). Number average length and diameter is 25 μm and 56 nm respectively. Total population is 146 for diameter measurements and 158 for length measurements.

² Certain equipment, instruments or materials are identified in this paper in order to adequately specify the experimental details. Such identification does not imply recommendation by the National Institute of Standards and Technology nor does it imply the materials are necessarily the best available for the purpose.

properties, thus we set up protocols that can isolate the effects of each step. There are three basic protocols: (1) *Squeeze*, this is the basic loading step in which the sample is placed between parallel plates, heated to the set temperature (200 °C) and then squeezed by the plates. During squeezing the sample spreads radially outward as the two parallel plates are compressed from (250 to 100) μm at a speed of 1 $\mu\text{m/s}$. The sample is then thermally quenched. (This protocol isolates the effects of sample loading. (2) *Shear*, in which the sample is loaded as above, sheared at a given rate for a period of 5 min (2 min for the case of $\dot{\gamma} = 100 \text{ s}^{-1}$) and then quenched. (3) *Shear then anneal*, in which the sample is loaded and sheared as above, but then annealed at the set temperature for 20 min before quenching. In the quenching step, the sample is cooled from the set temperature to below T_g of PS ($\approx 100 \text{ }^\circ\text{C}$) in approximately 2 min. Following quenching, the sample is removed for subsequent confocal microscopy, electron microscopy and electrical conductivity measurements. Sample thicknesses were measured again post annealing with a micrometer (Mitutoyo, resolution 1 μm).

During the shearing and annealing, the MWCNT nanocomposite was monitored via conventional optical microscopy with a long working distance objective. While individual nanotubes cannot be resolved due to the limited spatial resolution, the overall flow of the nanotube network was visible; this was used to track residual flow during annealing.

2.3. Electrical conductivity

For the electrical measurements, ohmic contacts were made with gold electrodes. The gold electrodes, with a diameter of 3.0 mm and a thickness of 0.1 μm , were evaporated in vacuum on both sides of the composite films. The thickness of the films was between 60 μm and 110 μm , measured with an uncertainty of $\pm 1 \mu\text{m}$. To avoid oxygen doping and moisture contamination all samples were handled either under a nitrogen or argon inert-gas atmosphere in a dry box. The measurements were carried out at isothermal conditions at room temperature. During the measurements, the specimen temperature was controlled to within $\pm 0.5 \text{ K}$. The direct constant current (DC) conductivity σ was determined from the linear and symmetric current–voltage I – V characteristics measured by sourcing a small current using a Keithley-6360 source meter. The current was increased in steps, each having duration of about 2 s. The conductivity was determined from the slope of the I – V plots, $I = \sigma(A/d)V$, where d is the sample thickness and A represents the area of the top electrode. The voltage drop maximum was kept within $\pm 1 \text{ V}$. Note that the direction of conductivity measurement is in the flow-gradient direction.

2.4. 3D imaging and image analysis

We utilize confocal microscopy in conjunction with open source image analysis software to obtain, manipulate and analyze the nanotube networks. We choose an optical microscopy method to study the networks rather than 3D TEM, because the nanotube density is sufficiently low, and the average nanotube length is sufficiently high that only the former method is feasible. Confocal microscopy (Leica, TCS SP5) was used in a non-fluorescent mode to build up three dimensional images from 51 slices, each of 500 nm thickness. The real and imaginary index of refraction of the CNTs limits the distance into the sample over which we are confident that we can perform quantitative image analysis to approximately 25 μm (this value is concentration dependent) which is less than the typical sample thickness of 70 μm . However, given the symmetry of the shear field and the absence of gravitational effects in this viscous polymer, we do expect the sample is symmetric about the mid-point and thus our measurements are representative of

most of the sample volume. Further, qualitative observations from slices at the mid-point between the top and bottom surfaces of the sample indicate that the structures are similar to those closer to the surface.

The x – y field of view is (246 \times 246) μm and the voxel dimensions are (240 \times 240 \times 500) nm. Fig. 2a shows a stack of such images that is constructed from the slices. These stacks are then reconstructed into 3D images via Fiji, an image processing package which is a distribution of ImageJ (NIH, v1.45b) combined with Java, Java 3D and user plugins organized into a coherent menu structure. Three of the plugins used from the Fiji package are summarized in Table 1. We extract statistical cluster information via use of open source 3D image analysis packages (ImageJ, NIH, v1.45b) [25,26] including *ImageJ 3D Viewer*, *3D object counter* [27] and *Skeleton3D/Analyze Skeleton* [28].

The image analysis proceeds through several steps. First, confocal microscopy images must be cleaned by a 3D filtering routine such as *Median3D* or *Smoothing3D* which reduces noise in the images, as shown in Fig. 2b. Next, as shown in Fig. 2c, a thresholding step (*Segmentation of 3D object*) is carried out to extract the objects from the background image. We note that this optical technique is capable of resolving the existence, length and position of the MWCNTs, but not their diameters – the tubes appear to have a diameter of approximately 250 nm, corresponding to the microscope point-spread function. Thus, a skeletonization

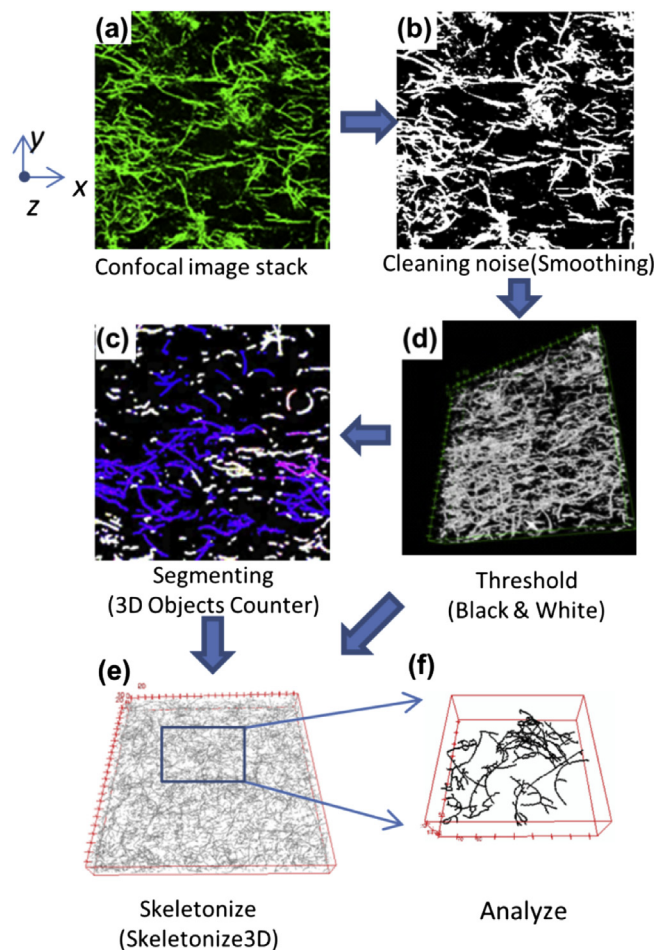


Fig. 2. Image analysis process from the initial stack of images (a) to the skeletonized image (e). In (f), all nanotubes except those belonging to the largest cluster are digitally removed from the image. Measure of one tick of the bounding box is 10 μm .

Table 1
Fiji plugins and menu for the image analysis in this study.

Plugin/menu name	Description	Author	Year	Ref.
Skeleton 3D/analyze skeleton	3D thinning and skeletonizing of 3D objects. Output: Detail branch information.	Ignacio Arganda-Carreras	2008–2012	[28]
3D object counter	Segmenting of 3D objects. Output: Volume, surface etc.	Fabrice P. Cordelières	2005–2007	[27]
Directionality	Analyze directionality distribution Output: the amount of 2D structures in a given direction.	Jean-Yves Tinevez	2010	[29]

step – *Skeleton3D* – is utilized as shown in Fig. 2e. The *Analyze Skeleton* plugin then tags all pixel/voxels in a skeleton image and counts all its junctions, branches and measures their average and maximum length. From the results of *Analyze Skeleton3D*, the size histogram of MWCNT clusters can be plotted based on the total branch length of each 3D branch cluster (ranging from $\approx 8 \mu\text{m}$ to $100 \mu\text{m}$), which is identified as one 3D object by this plugin. This is the central plugin used in this work for the analysis of MWCNT dispersion in a PS matrix. The plugin, *3D Object Counter* was used to verify the segmented results of *Analyze Skeleton3D* (Fig. 2d). We analyze the orientation distribution by the *Directionality* function which provides the orientation angle of the MWCNTs in the x – y plane (the flow/vorticity plane). The *Directionality* analysis produces an averaged orientation distribution of all 51 slices, expressed as one radar chart.

Fig. 2f shows an image of one cluster – the largest one – extracted from the image of Fig. 2e through the methods described above. As a check on the methods described above, we modified parameters in the plugins, such as thresholding values, in order to understand the sensitivity of the results to minor changes in these parameters. We found that the primary results of the paper, e.g., the power law relationships, were essentially unchanged.

We note that a nanotube is defined to be a member of a given cluster if any part of that nanotubes occupies the same voxel as another nanotube in that cluster. Due to the optical resolution limitations, we do not know if two adjacent nanotubes are in physical contact, but we can state that they are within approximately 500 nm of each other. As mentioned above, this length far exceeds the estimated distance of about 10 nm for nanotube–nanotube tunneling. Thus, the clusters that we define based on our optical method do not correspond exactly to the electrical ones. Even with TEM, in a three-dimensional cluster it is difficult to

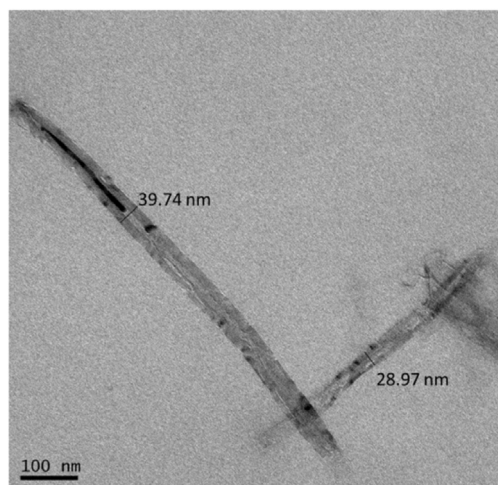


Fig. 3. TEM image showing a junction point between two MWCNTs.

measure the exact distance between nanotubes in a junction since a TEM image is a two-dimensional projection. A typical TEM micrograph shows a region of two overlapping nanotubes within the composite (Fig. 3). For this TEM, samples of the nanocomposites were also prepared by ultramicrotomy using an oscillating diamond knife (DIATOME®, 35°, Ultrasonic). Imaging was performed at an operating voltage of 80 kV for the composite.

3. Results

We use the *squeeze* protocol to determine the concentration at which the sample becomes electrically percolating. The left panel of Fig. 4 shows this occurs at approximately 0.1% by mass where the relatively high conductivity $\approx 10^{-7}$ (S/cm) is observed. Upon application of the *shear* protocol (middle panel) this high conductivity is maintained at the lowest shear rate of 0.1 s^{-1} , but a precipitous drop in conductivity occurs as the shear rate is progressively increased up to $\approx 10 \text{ s}^{-1}$ and beyond. Upon application of the *shear then anneal* protocol ($\dot{\gamma} = 100 \text{ s}^{-1}$) (right panel) we observe a recovery of conductivity. These observations are broadly similar to those described in the previous studies [6,13] where it has been attributed it to a shear induced rearrangement of the CNT conducting network structure that forms through a combination of direct MWCNT–MWCNT interactions.

We analyze the 3D images for their plethora of data regarding the MWCNT networks. The first metric we use to characterize the networks is the relative population of clusters of a given mass. We plot the mass distribution for several different MWCNT concentrations for squeezing flow in Fig. 5A. In these plots, *relative frequency* indicates the numbers of times a cluster within a given mass bin was observed divided by the total number of clusters within a

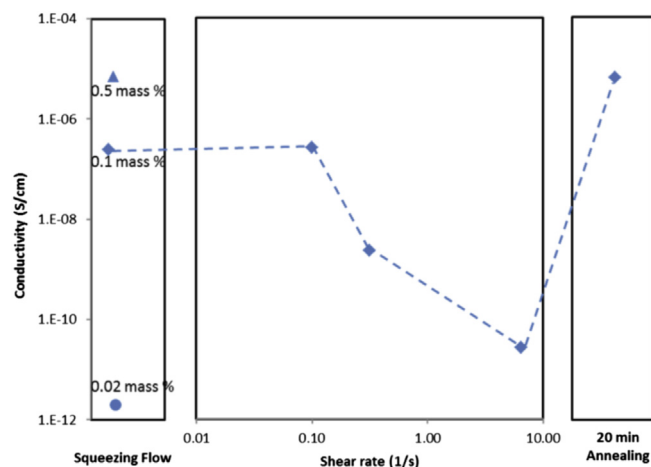


Fig. 4. Bulk electrical conductivity as a function of processing operation (squeezing shearing; and annealing) for the 0.1% mass fraction. For squeezing flow, two additional mass fractions (0.02% and 0.5%) are shown. Measurement uncertainty is less than the size of the data markers.

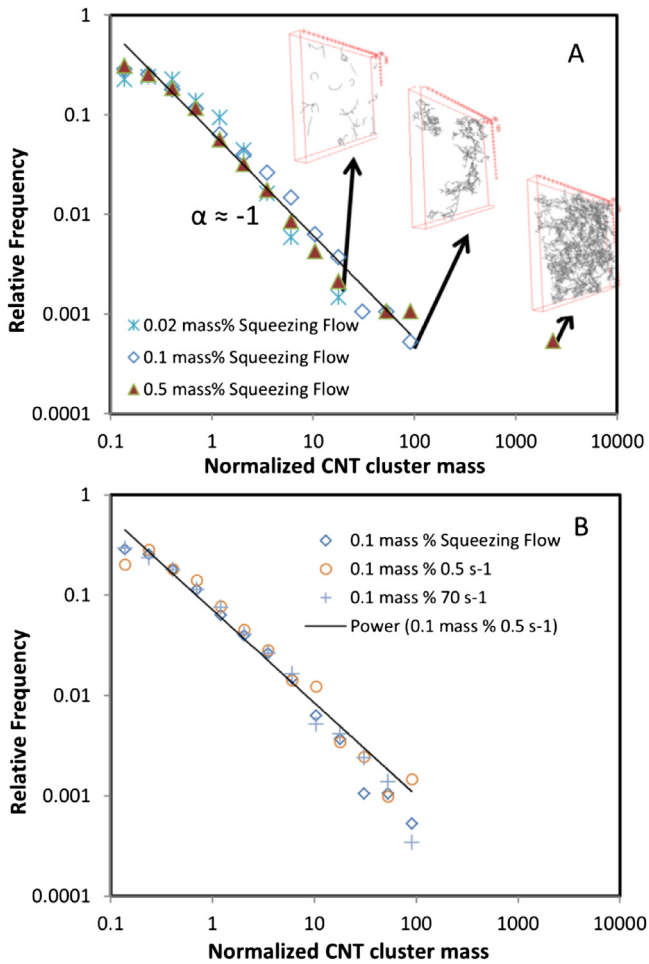


Fig. 5. Cluster size distributions for three different CNT compositions (A) and different stages of processing conditions (B). The vertical axis represents the probability of finding a cluster of a given relative mass. The arrows (A) show the cluster dispersion containing in the largest data (bin) for three different MWCNT concentrations. Bounding box volume is $(246 \times 246 \times 25) \mu\text{m}$.

3D image. *Normalized CNT cluster mass* then represents the total length of MWCNTs in a cluster divided by the average length of a MWCNT ($25 \mu\text{m}$). (Equivalently we could use the term *Normalized CNT cluster length*). Fig. 5A shows the power law relations for samples with MWCNT concentrations of 0.02%, 0.1% and 0.5% by mass, chosen so that they bracket the percolation point of approximately 0.1%. The data points towards the upper left of the plots whose normalized cluster mass is one or less are indicative of clusters that consist of only one nanotube. (The normalized CNT cluster mass can be less than one because of the broad distribution of MWCNT lengths, for example a relatively short isolated nanotube would have such a low normalized CNT cluster mass.) The data points on the lower right indicate the largest clusters, the three arrows indicate the maximum observed cluster mass for each concentration.

In experiments on melt-sheared polymer nanocomposites, one must be cognizant of reports of nanotube breakage during processing in twin-screw extruders and batch roller mixers, where intensive shear and extensional forces are generated in the narrow spaces where the screws and rollers come into closest contact with the walls or with each other [30,31]. In those reports, the resulting shorter nanotube length distributions decreased the conductivity and increases the concentration necessary to cause percolation. In our experiments (See Fig. 4) following our highest shear rate, the

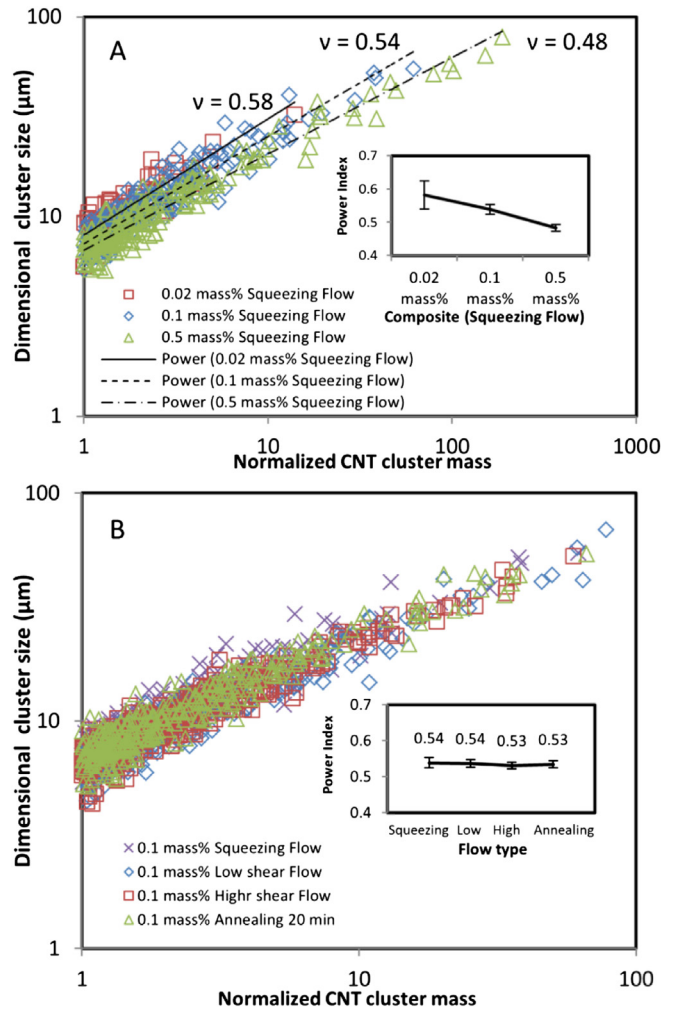


Fig. 6. Dimensional Cluster size vs. Cluster CNT length; (A) CNT composition effect: Inset shows the effect of the CNT composition of the nanocomposite on the power law index. Uncertainty is the standard deviation of the power index of a curve fitting. (B) Flow condition effect of 0.1% mass fraction CNT composite.

electrical conductivity returns to more than its original value after annealing. This would not occur if breakage was significant. Further, in the optical images, we do not see obvious decreases in the length distribution. In the simple-shear and gentle squeezing protocols employed here we thus find that breakage is not a significant occurrence.

An important observation is that these curves follow a power law of slope $\alpha \approx -1$ over a broad range of cluster sizes. This indicates that most clusters consist of a small number of MWCNTs, with larger clusters becoming progressively less likely. The normalized cluster distribution coincides with the predicted cluster distribution by a classical percolation theory [32] below percolation point. The largest clusters, though few in number, are critical because only those that span the sample can carry the DC electrical current. For the case of the 0.5% mass fraction, the lower right data point (the most massive cluster) falls off of the power law curve. We note that this data point represents one cluster (thus it is the smallest non-zero value of the relative frequency), and it contains over half the nanotubes in the sample image. It is thus representative of the case where finite sample and image size cuts off the distribution from its power law structure. The maximum cluster mass, as indicated by the arrows, is a strong function of concentration and the inset images show the largest clusters for each such

concentration. For example the maximum mass cluster for the 0.5% mass fraction sample is approximately 100 times greater than for the 0.02% sample.

Fig. 5B shows the power law relations for samples at the percolation concentration (0.1% mass fraction) but with three different processing protocols (i) *squeeze* (ii) *shear* ($\dot{\gamma} = 0.5 \text{ s}^{-1}$) and (iii) *shear* ($\dot{\gamma} = 70 \text{ s}^{-1}$). We selected the mass fraction of 0.1% because it is at the point of percolation and is thus highly sensitive to shear and shows conductivity that varies strongly with processing conditions. We expected to find that the decrease of conductivity following application of shear would manifest itself in the destruction of large clusters. However, the cluster distributions we measured following the different shear rates were relatively unaffected by the processing. This indicates that the power law cluster distribution that we have uncovered with our 3D data analysis method is robust, an important result for nanocomposite processing.

The size of the clusters as a function of their mass is important because in order for the conductive pathways to exist from one end of a sample to another at low mass fraction, the nanotubes clusters must be ramified. Fig. 6 shows a plot of the CNT cluster size s versus the normalized CNT mass, m . Here we define the size s as the cube root of the volume of the right rectangular prism that bounds a given cluster (as extracted from the *Analyze Skeleton3D* plugin). We again find a power law relation, $s(\text{cluster}) \sim \langle m \rangle^\nu$ where $1/\nu$ is the fractal or mass scaling dimension. The exponent ν decreases from 0.58 to 0.48 with increasing CNT concentration. We also find that the maximum cluster size increases rapidly as the concentration increases from below to above the percolation point; this is analogous to the increase in cluster mass with concentration that was described previously. The trend of decreasing power law exponent is reasonable, for example, a solid slug of nanotubes (volume fraction of unity), the exponent ν would be $1/3$. Fig. 6B shows the effect of different processing conditions at a constant concentration of 0.1% mass fraction. Similar to the observations of the cluster mass distribution (Fig. 5A), processing again had little effect on the observed cluster size.

The MWCNTs associate into clusters having a ramified, or branched network-like structure, a phenomenon previously identified in light scattering studies of CNT nanocomposites [33]. We can quantify the diffuse geometry of these clusters by determining their apparent fractal dimension and by making comparison to branched polymeric clusters encountered frequently in material science. Curiously, the change in ν values indicated in Fig. 6 is consistent with the associating clusters of particles forming linear polymer chains where ν ranges from 0.588 to 0.5 with increasing concentration [34,35]. This observation contrasts with the expected ν crossover between 0.5 and 0.40 for associating particle clusters forming branched particle clusters at equilibrium, i.e., lattice animals (swollen equilibrium branched polymers) and percolation clusters (equilibrium branched polymers with screened excluded volume interactions) [36,37]. It seems possible that the lateral association between the CNTs might inhibit branching to explain the closer similarity of our results to linear chain association. This suggestion requires further investigation however.

We next examine the effect of orientation distribution of the MWCNTs in a network and show the results from three separate protocols (defined in the Experimental section): (i) *squeeze* (ii) *shear* ($\dot{\gamma} = 100 \text{ s}^{-1}$) and (iii) *shear* ($\dot{\gamma} = 100 \text{ s}^{-1}$) then *anneal*. The average shear and extensional rates of the squeezing flow were calculated based on a Newtonian fluid assumption [38]. We see that the outward squeezing flow induces orientation in the radial direction (Fig. 7A), and that the imposed shear flow shifts the alignment to the shear direction (Fig. 7B). Interestingly, we see that following 20 min of annealing, the orientation becomes isotropic

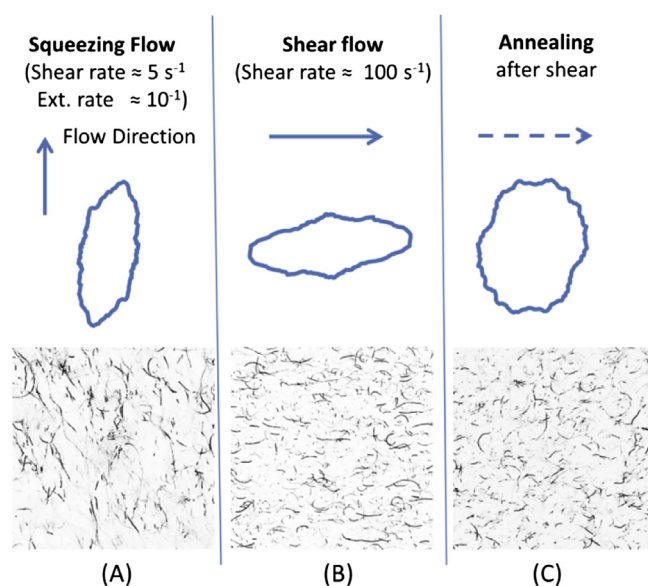


Fig. 7. x - y plane orientation distributions of MWCNTs showing the effect of flow type and annealing. Plots of ellipsoids represent orientation radar charts, bottom photos are bright field micrographs.

(Fig. 7C). While the MWCNT orientation distribution is a strong function of the processing parameters, we find that the orientational distribution alone does not determine the conductivity. For example the squeezed and sheared samples have similar orientation distributions (in different directions), but exhibit very different conductivities. We note that these radar plots are in the plane containing the flow and the vorticity (sometimes called neutral) axes whereas the conductivity is measured in the flow gradient direction. Thus there should not be a direct relationship between the orientation measured here and the conductivity. The orientation of the nanotubes is predominately in this flow – vorticity plane, but is not quantified in this work.

We further explore the invariance of the power law distribution to shearing by focusing attention on the very largest clusters, those that are believed to carry the DC current. In Fig. 8, we show only the largest cluster for each shear rate, by digitally subtracting out the other smaller clusters. While there are some changes in cluster size that are visible across the three conditions, these effects are subtle and do not obviously explain the four orders of magnitude difference in conductivity as the sample is processed.

Finally we examine the well-known phenomena [14] of conductivity recovery during annealing. As seen in Fig. 4, the conductivity recovers to a value slightly higher than the starting one after annealing. We compare the residual flow for two distinct experimental protocols; *shear vs. shear then anneal*. As seen in Fig. 9, the annealed sample exhibits a far greater residual shear rate at any given time in the annealing process (and far greater total strain). We have not identified the exact source of the residual flow; there could be several sources (temperature gradients, residual stress in the polymer and/or MWCNT network, non-parallelism of the plates). However, there will always be some residual flow in polymeric systems of this type.

This residual stress-induced flow may be a key component of the recovery of conductivity during annealing in the current experiments, and possibly for other reports as well. As mentioned earlier, it is known that conductivity decreases as a function of increasing shear. Further, recovery of conductivity is observed when a two-stage protocol is employed whereby the sample is first sheared at high rates (destroying conductivity) and followed by

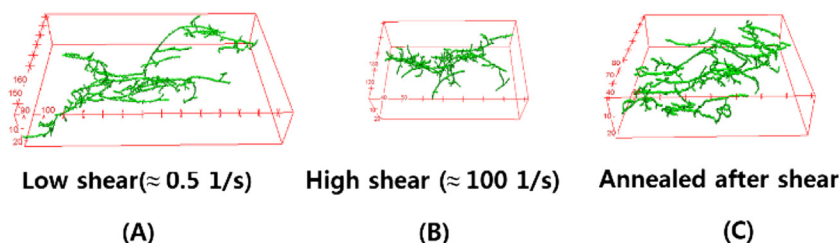


Fig. 8. Largest cluster observed following the indicated protocols. Measure of one tick of the bounding box is 10 μm .

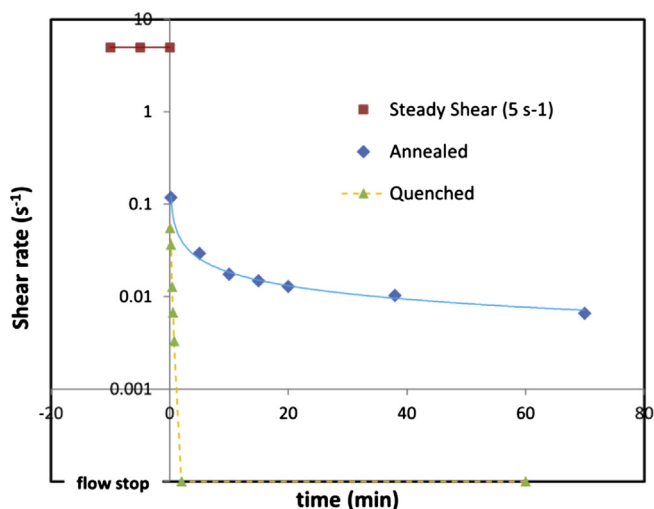


Fig. 9. Shear rate vs. annealing time. After cessation of the flow cell, still there is a residual flow. Quenching curve is included for the comparison; total shear strain is less than 120% while it is 3000% for the residual flow during 20 min. Uncertainty is less than the size of the data points.

shear at a significantly lower shear rate where the conductivity returns. Alig and coworkers report that clusters develop during annealing as well as during the second stage of their protocol. But what drives the re-orientation and reconfiguration of the MWCNTs? Our results suggest that during annealing there is residual flow, and we hypothesize that this flow is responsible for the changes in MWCNT orientation that lead to conductivity recovery. Our results do not however capture the small scale changes in network structure that seem to accompany the conductivity recovery process. These rearrangements probably occur at the interfacial scale about the CNT where small changes in the particle positions can be expected to lead to large changes in the contact resistances between the CNTs or between CNTs and quartz surfaces.

4. Conclusions

The measurement of the three dimensional structure of MWCNT networks over volumes encompassing thousands of nanotubes provides important insights into the effects of processing on nanocomposite properties. Our results indicate the formation of clusters whose size and size distribution exhibit power laws with cluster mass. These scaling laws are robust with respect to changes in concentration and processing conditions. In the current experiments, the cluster scaling does not correlate with changes in conductivity. This indicates that a subtle transformation has occurred within the clusters from a conducting to non-conducting state. This indicates that more subtle structural effects can be at play in determining conductivity, for example nanotube–nanotube

contact distances, which are not measured by these experiments, or perhaps shear-induced nanotube deletion zones at the surface of the polymer. Further work is needed to obtain detailed measurements of the orientation in the flow-gradient direction. These are interesting areas for future exploration.

Acknowledgments

We acknowledge Dr. Joy Dunkers for assistance in the use of laser scanning microscopy, Renu Sharma for TEM and Alex Liddle for critical discussions.

References

- [1] Coleman JN, Khan U, Gun'ko YK. Mechanical reinforcement of polymers using carbon nanotubes. *Adv Mater* 2006;18:689–706.
- [2] Xu YS, Ray G, Abdel-Magid B. Thermal behavior of single-walled carbon nanotube polymer-matrix composites. *Compos Pt A-Appl Sci Manuf* 2006;37:114–21.
- [3] Ounaies Z, Park C, Wise KE, Siochi EJ, Harrison JS. Electrical properties of single wall carbon nanotube reinforced polyimide composites. *Compos Sci Technol* 2003;63:1637–46.
- [4] Hwang TY, Kim HJ, Ahn Y, Lee JW. Influence of twin screw extrusion processing condition on the properties of polypropylene/multi-walled carbon nanotube nanocomposites. *Korea-Aust Rheol J* 2010;22:141–8.
- [5] Villmow T, Pegel S, Poetschke P, Wagenknecht U. Influence of injection molding parameters on the electrical resistivity of polycarbonate filled with multi-walled carbon nanotubes. *Compos Sci Technol* 2008;68:777–89.
- [6] Obrzut J, Douglas JF, Kharchenko SB, Migler KB. Shear-induced conductor-insulator transition in melt-mixed polypropylene-carbon nanotube dispersions. *Phys Rev B* 2007;76:195420.
- [7] Eken AE, Tozzi EJ, Klingenberg DJ, Bauhofer W. A simulation study on the effects of shear flow on the microstructure and electrical properties of carbon nanotube/polymer composites. *Polymer* 2011;52:5178–85.
- [8] Bauhofer W, Schulz SC, Eken AE, Skipa T, Lellinger D, Alig I, et al. Shear-controlled electrical conductivity of carbon nanotubes networks suspended in low and high molecular weight liquids. *Polymer* 2010;51:5024–7.
- [9] Kashiwagi T, Fagan J, Douglas JF, Yamamoto K, Heckert AN, Leigh SD, et al. Relationship between dispersion metric and properties of PMMA/SWNT nanocomposites. *Polymer* 2007;48:4855–66.
- [10] Haggenueller R, Fischer JE, Winey KI. Single wall carbon nanotube/polyethylene nanocomposites: nucleating and templating polyethylene crystallites. *Macromolecules* 2006;39:2964–71.
- [11] Abbasi S, Carreau PJ, Derdouri A. Flow induced orientation of multiwalled carbon nanotubes in polycarbonate nanocomposites: rheology, conductivity and mechanical properties. *Polymer* 2010;51:922–35.
- [12] Alig I, Skipa T, Lellinger D, Biedel M, Meyer H. Dynamic percolation of carbon nanotube agglomerates in a polymer matrix: comparison of different model approaches. *Phys Status Solidi B-Basic Solid State Phys* 2008;245:2264–7.
- [13] Alig I, Pötschke P, Lellinger D, Skipa T, Pegel S, Kasaliwal GR, et al. Establishment, morphology and properties of carbon nanotube networks in polymer melts. *Polymer* 2012;53:4–28.
- [14] Bauhofer W, Kovacs JZ. A review and analysis of electrical percolation in carbon nanotube polymer composites. *Compos Sci Technol* 2009;69:1486–98.
- [15] Kharchenko SB, Douglas JF, Obrzut J, Grulke EA, Migler KB. Flow-induced properties of nanotube-filled polymer materials. *Nat Mater* 2004;3:564–8.
- [16] Schueler R, Petermann J, Schulte K, Wentzel HP. Agglomeration and electrical percolation behavior of carbon black dispersed in epoxy resin. *J Appl Polym Sci* 1997;63:1741–6.
- [17] Eken AE, Tozzi EJ, Klingenberg DJ, Bauhofer W. A simulation study on the combined effects of nanotube shape and shear flow on the electrical percolation thresholds of carbon nanotube/polymer composites. *J Appl Phys* 2011;109:084342-1–084342-9.
- [18] Li C, Thostenson ET, Chou T-W. Dominant role of tunneling resistance in the electrical conductivity of carbon nanotube-based composites. *Appl Phys Lett* 2007;91.

- [19] Hobbie EK, Wang H, Kim H, Lin-Gibson S, Grulke EA. Orientation of carbon nanotubes in a sheared polymer melt. *Phys Fluids* 2003;15:1196–202.
- [20] Pujari S, Rahatekar S, Gilman JW, Koziol KK, Windle AH, Burghardt WR. Shear-induced anisotropy of concentrated multiwalled carbon nanotube suspensions using x-ray scattering. *J Rheol* 2011;55:1033–58.
- [21] Fry D, Langhorst B, Wang H, Becker ML, Bauer BJ, Grulke EA, et al. Rheo-optical studies of carbon nanotube suspensions. *J Chem Phys* 2006;124.
- [22] Galindo-Rosales FJ, Moldenaers P, Vermant J. Assessment of the dispersion quality in polymer nanocomposites by rheological methods. *Macromol Mater Eng* 2011;296:331–40.
- [23] Tsarouchas D, Markaki AE. Extraction of fibre network architecture by X-ray tomography and prediction of elastic properties using an affine analytical model. *Acta Mater* 2011;59:6989–7002.
- [24] Singh C, Shaffer MSP, Koziol KKK, Kinloch IA, Windle AH. Towards the production of large-scale aligned carbon nanotubes. *Chem Phys Lett* 2003;372:860–5.
- [25] Philippe A, Thomas B. 3d Image processing and analysis with ImageJ [ImageJ Documentation Wiki]; 2010.
- [26] Wayne R. ImageJ <http://rsbweb.nih.gov/ij/index.html>; 2012.
- [27] Cordelires F, Jackson J. 3D object counter <http://rsbweb.nih.gov/ij/plugins/track/objects.html>; 2007.
- [28] Arganda-Carreras I, Fernández-González R, Muñoz-Barrutia A, Ortiz-De-Solorzano C. 3D reconstruction of histological sections: application to mammary gland tissue. *Microsc Res Tech* 2010;73:1019–29.
- [29] Tinevez J-Y. Directionality – Fiji <http://fiji.sc/Directionality>; 2010.
- [30] Castillo FY, Socher R, Krause B, Headrick R, Grady BP, Prada-Silvy R, et al. Electrical, mechanical, and glass transition behavior of polycarbonate-based nanocomposites with different multi-walled carbon nanotubes. *Polymer* 2011;52:3835–45.
- [31] Guo J, Liu Y, Prada-Silvy R, Tan Y, Azad S, Krause B, et al. Aspect ratio effects of multi-walled carbon nanotubes on electrical, mechanical, and thermal properties of polycarbonate/MWCNT composites. *J Polym Sci Part B* 2014;52:73–83.
- [32] Genin D. Percolation: theory and application; 2007. www.nist.gov/itl/cxs/upload/percolation_slides.pdf.
- [33] Chatterjee T, Jackson A, Krishnamoorti R. Hierarchical structure of carbon nanotube networks. *J Am Chem Soc* 2008;130. 6934–+.
- [34] Ammon Aharony. Introduction to percolation theory Dietrich Stauffer. n.d.
- [35] Douglas JF. Swelling and growth of polymers, membranes, and sponges. *Phys Rev E* 1996;54:2677–89.
- [36] Rouault Y, Milchev A. Monte-carlo study of living polymers with the bond-fluctuation method. *Phys Rev E* 1995;51:5905–10.
- [37] Rouault Y, Milchev A. Monte Carlo study of the molecular-weight distribution of living polymers. *Phys Rev E* 1997;55:2020–2.
- [38] Engmann J, Servais C, Burbidge AS. Squeeze flow theory and applications to rheometry: a review. *J Nonnewton Fluid Mech* 2005;132:1–27.